Automatic detection of endothelial cells in 3D angiogenic sprouts from experimental phase contrast images

Automatic Detection of Endothelial Cells in 3D Angiogenic Sprouts from Experimental Phase Contrast Images

Mengmeng Wang[a,b], Lee-Ling Sharon Ong[a], Justin Dauwels[a,b], H. Harry Asada[a,c]

[a]Singapore-MIT Alliance for Research and Technology, Singapore;
[b]School of Electrical and Electronic Engineering, Nanyang Technological University, Singapore;
[c]Department of Mechanical Engineering, MIT Cambridge, MA, USA

ABSTRACT

Cell migration studies in 3D environments become more popular, as cell behaviors in 3D are more similar to the behaviors of cells in a living organism (in vivo). We focus on the 3D angiogenic sprouting in microfluidic devices, where Endothelial Cells (ECs) burrow into the gel matrix and form solid lumen vessels. Phase contrast microscopy is used for long-term observation of the unlabeled ECs in the 3D microfluidic devices. Two template matching based approaches are proposed to automatically detect the unlabeled ECs in the angiogenic sprouts from the acquired experimental phase contrast images. Cell and non-cell templates are obtained from these phase contrast images as the training data. The first approach applies Partial Least Square Regression (PLSR) to find the discriminative features and their corresponding weight to distinguish cells and non-cells, whereas the second approach relies on Principal Component Analysis (PCA) to reduce the template feature dimension and Support Vector Machine (SVM) to find their corresponding weight. Through a sliding window manner, the cells in the test images are detected. We then validate the detection accuracy by comparing the results with the same images acquired with a confocal microscope after cells are fixed and their nuclei are stained. More accurate numerical results are obtained for approach I (PLSR) compared to approach II (PCA & SVM) for cell detection. Automatic cell detection will aid in the understanding of cell migration in 3D environment and in turn result in a better understanding of angiogenesis.

Keywords: Endothelial cell detection, 3D angiogenic sprouts, partial least square regression, phase contrast images

1. INTRODUCTION

Phase contrast microscopy, which converts phase shifts in light passing through a transparent specimen to brightness changes in the image, is widely used to observe long-term multi-cellular processes. We use phase contrast microscopy to study the behavior of endothelial cells (ECs), which line the interior of blood vessels. The growth of blood vessels from existing vessels is known as angiogenesis, a critical process in growth, development and cancer invasion.[1] We conduct angiogenic experiments in microfluidic devices[2] and image the sprouts and vascular networks formed by ECs in 3D gel matrix daily over a period of 10 to 14 days.

Accurate cell detection from the experimental images will aid in the understanding of cell migration in the 3D environment and the angiogenic process. In this paper, we propose two automated image processing algorithms to detect the ECs in the angiogenic sprouts from our experimental phase contrast images. We validate the detection accuracy by comparing the detection results with the same images acquired with a confocal microscope after the cells are fixed and their nuclei are stained.

Different cells have different morphologies. Even for the same kind of cells, their shape vary when they are cultured using different assays. Fig. 1(a) provides an example of how cells look like on a 2D surface. Many existing approaches base on pixel intensity to detect cells on 2D surface from phase contrast images.[3–5] Ambriz-Colin et al. calculated the pixel intensity variance to distinguish the possible cell regions from the phase contrast image background.[3] Usaj et al. convolve an inverted Laplacian of Gaussian (LoG) with the image and pick the local extrema as cell centers.[4] However, these approaches that only exploit the pixel intensity are not applicable to the cases in which cells and background have similar intensity distributions. Active contour algorithm is another popular approach to segment cells in 2D environments from phase contrast images.[6,7] Bunyak et al. relied on a level set-based active contour algorithm that robustly handles a large number of cells.[7]

Further author information: (Send correspondence to Mengmeng Wang)
Mengmeng Wang: E-mail: mwang009@e.ntu.edu.sg, Telephone: +65 98309185

Medical Imaging 2015: Image Processing, edited by Sébastien Ourselin, Martin A. Styner, Proc. of SPIE Vol. 9413, 94132I · © 2015 SPIE · CCC code: 1605-7422/15/$18 · doi: 10.1117/12.2081819

Template matching find matches of a gray level template within a large gray level image, based on a "goodness" of match statistic evaluated at each pixel in the images.[8] Young et al. adopted it to detect cells on a 2D surface from differential interferen ce contrast (DIC) microscopy images.[9,10] Covariance and the mean square distance between the template and the part of the test image it overlaps act as the indicator of the "goodness" of match.

Machine learning methods, such as Support Vector Machines (SVMs), have been adopted to detect cells in 2D environments from microscopy images ranging from dark field images to fluorescent images.[11,12] Wei et al. developed two SVM-based classifiers to separate cells from background and then to distinguish live cells from dead ones in dark field images.[11] Wang et al. detected the stained cells based on both the intensity and shape information from fluorescent images.[12]

Only several approaches exist to detect cells in 3D environment.[13,14] Adanja et al. applied the local maximum filter to extract a large number of cells embedded in 3D volumes from phase contrast images (refer to Fig. 1(b)).[13] Dufour et al. segmented the fluorescent cells in 3D environment from confocal microscopy with coupled active surfaces.[14]

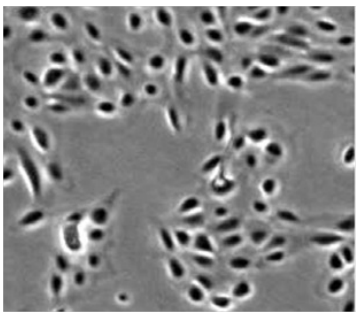

(a) Cell population on a 2D surface[7]

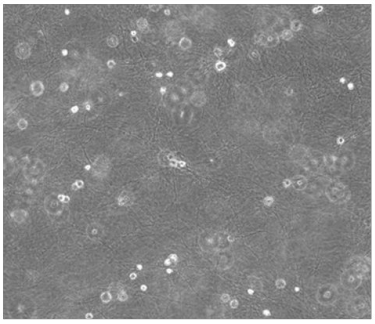

(b) Cells embedded in 3D gel[13]

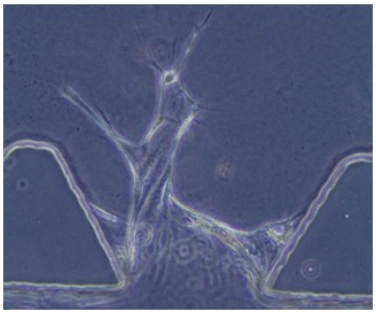

(c) Angiogenic sprouting cells in 3D gel

Figure 1. Image examples for cell detection.

We want to develop an algorithm to detect the Endothelial Cells (ECs) forming the angiogenic sprouts in 3D microfluidic devices from the acquired 2D phase contrast images, shown in Fig. 1(c). These ECs migrate at different depths, while we only have one 2D phase contrast slide. Some of the cells are out of focus unavoidably. To form the angiogenic sprouts, these ECs connect and interact with the gel and each other. They do not have clear boundaries compared with the cells in other conditions, which can be seen from Fig. 1. Thus it is more challenging to detect these angiogenic sprouting cells from the phase contrast images with low signal to noise ratios.

In this paper, we propose two automated image analysis algorithms to detect the angiogenic sprouting ECs from the experimental phase contrast images. To our knowledge, our novelty is that:

- we are the first to use Partial Least Square Regression (PLSR) as the indicator of "goodness" of matches for template matching for cell detection,
- we are the first to detect cells networks from phase contrast images,
- we use end-point confocal images to verify the cell detection results.

The structure of this paper is as follows. In Section II, we elaborate on our proposed approaches for automated cell detection. We present numerical results in Section III and offer concluding remarks in Section IV.

2. ENDOTHELIAL CELL DETECTION ALGORITHMS

We have developed two automated image processing algorithms to detect the ECs from the experimental phase contrast images through template matching. The flowchart of the template matching process is shown in Fig. 2. The first step is to extract the discriminative and reliable features for the input data through dimensionality reduction. The second step is to train a classifier based on the extracted discriminative features and the corresponding output data. Lastly, the resulting classifier will then be used to detect cells from the experimental phase contrast images through a sliding window approach.

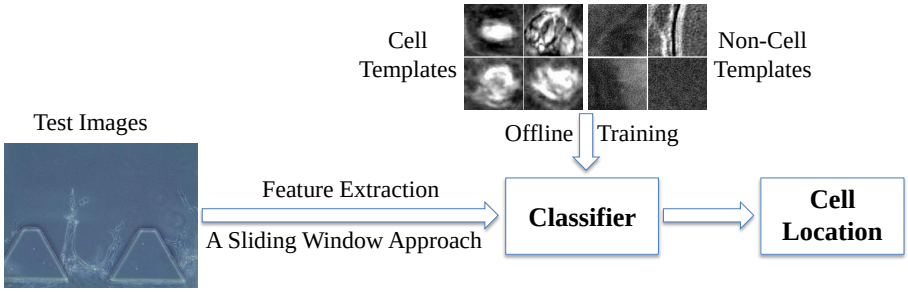

Figure 2. Template matching flowchart: offline training is used to train a classifier based on the extracted discriminative features from the training data. The classifier helps to sort each pixel in the test images to cells and non-cells through a sliding window approach.

We obtain the cell and non-cell templates, varying in size, from our experimental images. In order to capture only texture information, size information has to be removed. We take the desired template size to be the mean of all the templates to reduce the discrepancies obtained from scaling. For our dataset, the mean template size is 106×94. Each template is scaled to this value and is represented by a 106×94 matrix, in which each element is the gray level of the corresponding pixel. Each matrix is converted to a high dimensional vector $\mathbf{x}$. Each image is represented as: $y = +1$ for cell templates and $y = -1$ for non-cell templates. Then we obtain our training input and output as:

$$\mathbf{X} = [\mathbf{x}^1, \cdots, \mathbf{x}^N] \in \mathbb{R}^{m \times N}, \tag{1}$$

$$\mathbf{Y} = [y^1, \cdots, y^N] \in \mathbb{R}^{1 \times N}, \tag{2}$$

where superscripts $1, \cdots, N$ represents template number, each $\mathbf{x}$ is an m-dimensional vector, and each y is a binary value.

We propose two approaches for cell detection. The first approach employs PLSR for both dimensionality reduction and classification. The second approach applies PCA for dimensionality reduction and SVM for classification.

2.1 Approach I – PLSR

PLSR is a statistical method to find a low-dimensional set of input space variables that is most correlated with a given set of output data.[15] For the given set of input $\mathbf{X}$ and output $\mathbf{Y}$, the algorithm consists of three steps.

The first step is to calculate the most correlated latent variable $\mathbf{z}_1$. The unit vector $\mathbf{v}_1$, associated with this most correlated latent variable $\mathbf{z}_1$, is calculated by:

$$\mathbf{v}_1 = \arg\max_{\mathbf{v}} \mathbf{J}(\mathbf{v}) = \frac{\mathbf{X}\mathbf{Y}^T}{|\mathbf{X}\mathbf{Y}^T|}, \tag{3}$$

where $\mathbf{J}$ is the correlation between $\mathbf{X}$ and $\mathbf{Y}$, as shown in Fig. 3(a). Then the most correlated variable $\mathbf{z}_1 = \mathbf{X}^T\mathbf{v}_1 \in \mathbb{R}^{N \times 1}$.

The second step is to predict the output $\mathbf{Y}$ from the obtained latent variable $\mathbf{z}_1$ using linear prediction. For instance, the predicted output $\hat{y}^i$ for each template i is calculated by:

$$\hat{y}^i = c_1 z_1^i, \tag{4}$$

where c_1 is the scalar coefficient correlated with $\mathbf{z}_1$. It is calculated by minimizing the mean square error:

$$c_1 = \arg\min_{c} \sum_{i=1}^{N} (y^i - \hat{y}^i) = \frac{\mathbf{Y}\mathbf{z}_1}{\mathbf{z}_1^T\mathbf{z}_1}. \tag{5}$$

The third step is to examine the correlation between the input and output residues. Since $\mathbf{X}$ and $\mathbf{Y}$ may have correlation in other directions, the accuracy of the predicted output based on the single latent variable $\mathbf{z}_1$ is limited. We introduce another latent variable $\mathbf{z}_2$, which accounts for the prediction of the residue that $\mathbf{z}_1$ could not predict, to improve the accuracy. The input and output residues are calculated as:

$$\mathbf{X}' = \mathbf{X} - \mathbf{X}\frac{\mathbf{z}_1\mathbf{z}_1^T}{\mathbf{z}_1^T\mathbf{z}_1}, \tag{6}$$

$$\mathbf{Y}' = \mathbf{Y} - c_1\mathbf{z}_1^T. \tag{7}$$

The second latent variable $\mathbf{z}_2$ and its correlated coefficient c_2 can be determined by repeating the first two steps but replacing the input $\mathbf{X}$ and output $\mathbf{Y}$ with the new residues $\mathbf{X}'$ and $\mathbf{Y}'$ respectively.

We iterate the above steps until the correlation between the input and output residues diminishes to obtain a series of latent variables, $\mathbf{z}_1, \cdots, \mathbf{z}_{m^*}$ and their corresponding coefficients, $c_1, \cdots, c_{m^*}$. For one template i, the predicted output $\hat{y}^i$ is:

$$\hat{y}^i = c_1 z_1^i + \cdots + c_{m^*} z_{m^*}^i, \tag{8}$$

where m^* is the optimum number of PLS components and $z_1^i, \cdots, z_{m^*}^i$ are scalar latent variables for the template i. The percentage variance explained in the output variables, which is a function of the number of PLS components, works as the criteria to determine the optimum number of PLS component m^*. Our goal is to achieve 95% of the variance explained in the output variables, where $m^* = 4$ is selected in this paper from the relation shown in Fig. 3(b).

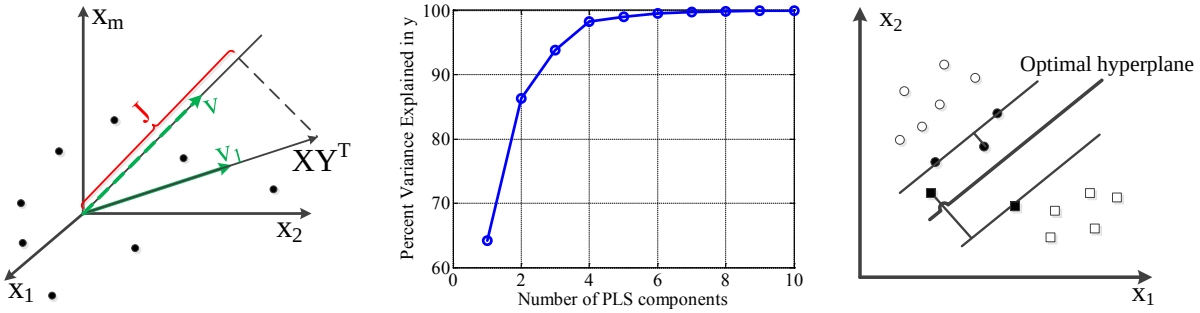

(a) (b) (c)

Figure 3. Diagrams to illustrate: (a) PLSR; (b) Percent of variance explained vs. the number of PLS components; and (c) SVM.

2.2 Approach II – PCA and SVM

In this approach, we firstly reduce our training input dimension by PCA and then train the SVM classifier to distinguish the cells from background.

PCA models the given variables by a smaller number of uncorrelated latent variables called principal components (PCs). We denote the covariance matrix of X by R, and the eigenvalues of R by $\lambda_1 \cdots \lambda_m$ in descending order. In order to select a suitable number of PCs, it is common practice to compute the cumulative percentage variance (CPV) as:

$$\text{CPV} = \frac{\sum_{j=1}^{n^*}\lambda_j}{\sum_{i=1}^{m}\lambda_i}, \tag{9}$$

where n^* is the number of PCs. We aim for a CPV of 95% and select n^* accordingly (typically $n^* = 4$).

SVM is then applied to find an optimal hyperplane to separate the dimension-reduced training data with a tolerable misclassification rate, as shown in Fig. 3(c). The decision function for the L1 soft-margin SVM is given by:[16]

$$D(\mathbf{x}_r^i) = w^T\mathbf{x}_r^i + b, \tag{10}$$

where $\mathbf{x}_r^i$ is the rth dimension-reduced template, w is the normal vector of the hyperplane and b is a bias term. To obtain the optimal hyperplane, we determine the values for w and b by solving the following optimization problem:

$$[w,b] = \arg\min_{w,b}\left(\frac{|w|^2}{2} + C\sum_{i=1}^{N}\xi_i\right), \tag{11}$$

$$\text{subject to } \; y^i(w^T\mathbf{x}_r^i + b) \geq 1 - \xi_i, \; \xi_i \geq 0, \tag{12}$$

where C is the margin parameter that determines the trade-off between the maximization of the margin and minimization of the classification error.[17]

After obtaining the trained classifier, the cells are detected from the experimental phase contrast images through a sliding window manner. The algorithms for both approaches are shown in Table 1.

Table 1. Cell detection algorithm for both approaches.

	Approach I	Approach II
Offline Training $\mathbf{X} \in \mathbb{R}^{m \times N}$ $\mathbf{Y} \in \mathbb{R}^{1 \times N}$	PLSR: $\mathbf{z}^i = \mathbf{x}^{iT}\mathbf{V}$ $\hat{\mathbf{y}}^i = \mathbf{c}\mathbf{z}^{iT}$ where $\mathbf{c} \in \mathbb{R}^{1 \times m^*}$, $\mathbf{V} = [\mathbf{v}_1, \cdots, \mathbf{v}_{m^*}] \in \mathbb{R}^{m \times m^*}$	PCA: $\mathbf{x}_r^i = \mathbf{U}^T\mathbf{x}^i$ SVM: $\hat{\mathbf{y}}^i = w^T\mathbf{x}_r^i + b$ where $\mathbf{U} = [\mathbf{u}_1, \cdots, \mathbf{u}_n] \in \mathbb{R}^{m \times n}$
Sliding Window Detection	Size of test image: $P \times Q$ Size of templates: $p \times q$ for $i = \frac{p}{2} : P - \frac{p}{2}$ and $j = \frac{q}{2} : Q - \frac{q}{2}$ $\mathbf{T}_{\text{temp}} = \mathbf{T}(i - \frac{p}{2} + 1 : i + \frac{p}{2}, j - \frac{q}{2} + 1 : j + \frac{q}{2})$ $\mathbf{T}'_{\text{temp}} = \text{reshape}(\mathbf{T}_{\text{temp}}, m, 1)$	
Cell Detection	$\hat{\mathbf{Y}}(i,j) = \mathbf{c}\mathbf{V}^T\mathbf{T}'_{\text{temp}}$	$\hat{\mathbf{Y}}(i,j) = w^T\mathbf{U}^T\mathbf{T}'_{\text{temp}} + b$
Decision Criteria	$\begin{cases} \text{Cell} & \text{if } \hat{\mathbf{Y}}(i,j) > 0 \\ \text{Non-Cell} & \text{Otherwise} \end{cases}$	

3. RESULTS

We provide two examples to illustrate our cell detection approaches. Fig. 4(a) and 4(d) show the cell detection results for approach I; Fig. 4(b) and 4(e) show the cell detection results for approach II, where the red stars $*$ indicate the location of cell nuclei. Fig. 4(c) and 4(f) are their corresponding 3D confocal images after fixed-cell staining with Hoechst dye (Invitrogen), which is a blue fluorescent stain specific for DNA. The blue blobs in the confocal images indicate the cell nuclei. We see that cell detection using approach I produces better results than approach II. To evaluate the performance of both approaches quantitatively, precision and recall measures are estimated. Generally, for a given classifier and a set of instances, a 2×2 confusion matrix (Table 2) can be constructed to represent the disposition of the set of instances.[18] Our actual positives and negatives are extracted from the 3D confocal images by visual inspection.

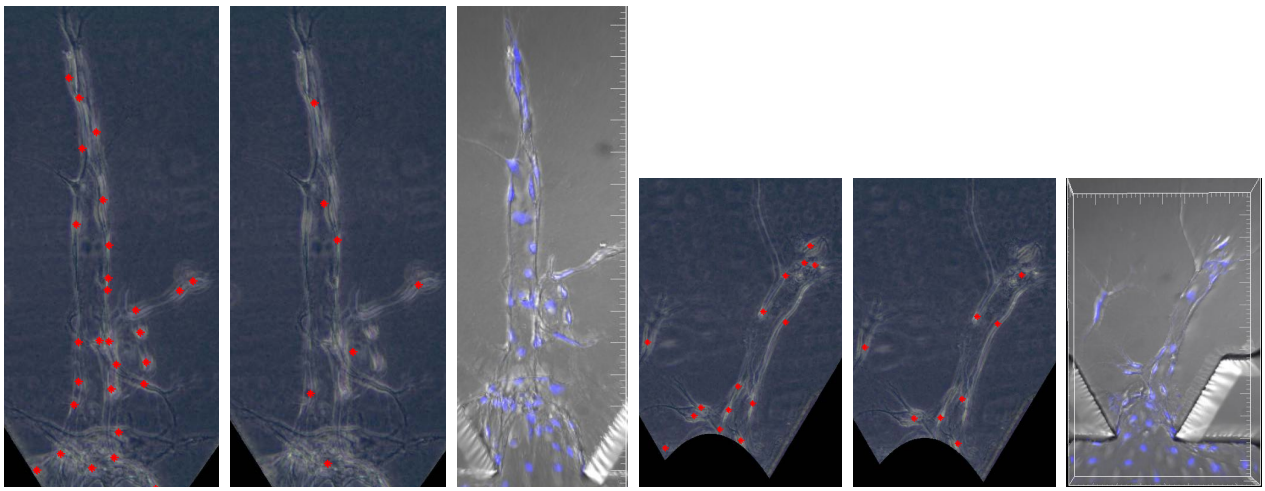

(a) Approach I (b) Approach II (c) Confocal images (d) Approach I (e) Approach II (f) Confocal images

Figure 4. Examples of cell detection results for both approaches and their corresponding confocal images: (a)(d) are the results of approach I and (b)(e) are the results of approach II, where the red stars $*$ indicate the location of cell nuclei; (c)(f) are their corresponding 3D confocal images, where the blue blobs indicate the stained cell nuclei.

Table 2. Confusion matrix for a binary classifier.

	Actual Positive	Actual Negative
Assigned Positive	True Positive (TP)	False Positive (FP)
Assigned Negative	False Negative (FN)	True Negative (TN)

Precision is the fraction of detected cells that are actual cells, whereas recall is the fraction of actual cells that are detected:

$$\text{Precision} = \frac{\text{TP}}{\text{TP+FP}}, \qquad \text{Recall} = \frac{\text{TP}}{\text{TP+FN}}. \tag{13}$$

Table 3 shows the confusion matrices of cell detection results for both approaches. For case 1, the actual positives and negatives are extracted from all the stacks of confocal images. Table 4 lists the corresponding precision and recall calculated based on (13). The precision for both approaches is above 80%, suggesting that most of the detected cells are actual cells. The recall for approach I is much higher than for the approach II, indicating that approach I detects most of the actual cells while approach II fails to do so. We hypothesize that PLS produces more specific set of variables to predict the given output data than PCA as PCA only explains the input instead of the relationship between the input and output data, whereas PLS addresses this issue by finding the PLS components that are most correlated with the given output.

The recall of PLSR is limited to about 81%, which can be explained as follows. The height of our device is 120*um* and there are cells migrating throughout this range. We only acquire 2D image of sprouts in focus. Some cells, which are external to the sprout, are out of focus and almost invisible in the phase contrast images. These cells are not detected by our algorithms. However, these out of focus cells are detected from the confocal images. Thus for case 2, our actual positives and negatives are from only one stack of the confocal images, which has the similar focal plane as the 2D phase contrast image. In this case, the recall increases to 90% for Approach I.

From the numerical results in Table 4, we conclude that approach I is a preferable algorithm for cell detection from experimental phase contrast images.

Table 3. Confusion matrix for both approaches.

		Case 1: All stacks		Case 2: One stack	
		Actual Positive	Actual Negative	Actual Positive	Actual Negative
Approach I	Assigned Positive	215	29	215	29
	Assigned Negative	51	12011496	23	12011524
Approach II	Assigned Positive	107	26	107	26
	Assigned Negative	159	12011499	131	12011527

Table 4. Classification performance of cell detection (in %).

	Case 1: All stacks		Case 2: One stack	
Cell Detection Approach	Precision	Recall	Precision	Recall
Approach I	88.11	80.83	88.11	90.34
Approach II	80.45	40.23	80.45	44.96

4. CONCLUSIONS

In this paper, we propose two automated image processing algorithms to detect cells embedded in 3D gel from our acquired phase contrast images through template matching. The first approach is based on PLSR, while the second approach mainly employs PCA & SVM. Numerical results from Section III have shown that PLSR is a more preferable algorithm for cell detection from experimental phase contrast images.

In the future, we will further improve the detection performance by introducing extra input features to the classifier and incorporating the sprouts information into cell detection.

ACKNOWLEDGMENTS

This research was supported by the National Research Foundation Singapore through the Singapore MIT Alliance for Research and Technologys BioSystems and Micromechanics Inter-Disciplinary Research programme.

REFERENCES

[1] Gerhardt, H., "Vegf and endothelial guidance in angiogenic sprouting," *VEGF in Development* , 68–78 (2008).

[2] Farahat, W., Wood, L., Zervantonakis, I., Schor, A., Ong, S., Neal, D., Kamm, R., and Asada, H., "Ensemble analysis of angiogenic growth in three-dimensional microfluidic cell cultures," *PloS one* **7**(5), e37333 (2012).

[3] Ambriz-Colin, F., Torres-Cisneros, M., Avina-Cervantes, J. G., Saavedra-Martinez, J. E., Debeir, O., and Sanchez-Mondragon, J. J., "Detection of biological cells in phase-contrast microscopy images," *Proceedings of the Fifth Mexican International Conference on Artificial Intelligence* , 68–77, IEEE Computer Society (2006).

[4] Usaj, M., Torkar, D., and Miklavcic, D., "Automatic cell detection in phase-contrast images for evaluation of electroporation efficiency in vitro," *11th Mediterranean Conference on Medical and Biomedical Engineering and Computing 2007* , 851–855, Springer (2007).

[5] Ersoy, I., Bunyak, F., Mackey, M. A., and Palaniappan, K., "Cell segmentation using hessian-based detection and contour evolution with directional derivatives," *Image Processing, 2008. ICIP 2008. 15th IEEE International Conference on* , 1804–1807, IEEE (2008).

[6] Padfield, D., Rittscher, J., Thomas, N., and Roysam, B., "Spatio-temporal cell cycle phase analysis using level sets and fast marching methods," *Medical image analysis* **13**(1), 143–155 (2009).

[7] Bunyak, F., Palaniappan, K., Nath, S., Baskin, T., and Dong, G., "Quantitative cell motility for in vitro wound healing using level set-based active contour tracking," *Biomedical Imaging: Nano to Macro, 2006. 3rd IEEE International Symposium on* , 1040–1043 (2006).

[8] Gonzalez, R. C. and Woods, R. E., [*Digital image processing*], Prentice hall Upper Saddle River (2002).

[9] Young, D. and Gray, A. J., "Template construction and matching for identification of cells in differential interference contrast microscope images," *Image Analysis and Interpretation, 1998 IEEE Southwest Symposium on* , 238–243, IEEE (1998).

[10] Young, D., Glasbey, C. A., Gray, A. J., and Martin, N. J., "Towards automatic cell identification in dic microscopy," *Journal of microscopy* **192**(2), 186–193 (1998).

[11] Wei, N., You, J., Friehs, K., Flaschel, E., and Nattkemper, T., "An in situ probe for on-line monitoring of cell density and viability on the basis of dark field microscopy in conjunction with image processing and supervised machine learning," *Biotechnology and bioengineering* **97**(6), 1489–1500 (2007).

[12] Wang, M., Zhou, X., Li, F., Huckins, J., King, R., and Wong, S., "Novel cell segmentation and online svm for cell cycle phase identification in automated microscopy," *Bioinformatics* **24**(1), 94–101 (2008).

[13] Adanja, I., Megalizzi, V., Debeir, O., and Decaestecker, C., "A new method to address unmet needs for extracting individual cell migration features from a large number of cells embedded in 3d volumes," *PloS one* **6**(7), e22263 (2011).

[14] Dufour, A., Shinin, V., Tajbakhsh, S., Guillén-Aghion, N., Olivo-Marin, J., and Zimmer, C., "Segmenting and tracking fluorescent cells in dynamic 3-d microscopy with coupled active surfaces," *Image Processing, IEEE Transactions on* **14**(9), 1396–1410 (2005).

[15] Abdi, H., "Partial least squares regression and projection on latent structure regression (pls regression)," *Wiley Interdisciplinary Reviews: Computational Statistics* **2**(1), 97–106 (2010).

[16] Abe, S., [*Support vector machines for pattern classification*], Springer (2010).

[17] Orsenigo, C. and Vercellis, C., "Discrete support vector decision trees via tabu search," *Computational statistics & data analysis* **47**(2), 311–322 (2004).

[18] Fawcett, T., "An introduction to roc analysis," *Pattern recognition letters* **27**(8), 861–874 (2006).